Particle Accelerators, Vol. 63, pp. 147–170
Reprints available directly from the publisher
Photocopying permitted by license only

CONSIDERATIONS ON THE DIFFRACTION LIMITATIONS TO THE SPATIAL RESOLUTION OF OPTICAL TRANSITION RADIATION

K. HONKAVAARA[a,b,*], X. ARTRU[c], R. CHEHAB[a] and A. VARIOLA[a,†]

[a]*Laboratoire de l'Accélérateur Linéaire, bat. 200, IN2P3-CNRS, Université de Paris-Sud, B.P. 34, F-91898 Orsay Cedex, France;* [b]*Helsinki Institute of Physics, University of Helsinki, P.O. Box 9, FIN-00014, Finland;* [c]*Institut de Physique Nucléaire de Lyon IN2P3-CNRS and Université Claude Bernard, F-69622 Villeurbanne Cedex, France*

(Received 17 November 1998; In final form 1 April 1999)

The interest in using optical transition radiation (OTR) in high energy (multiGeV) electron beam diagnostics has motivated theoretical and experimental investigations on the limitations brought by diffraction on the attainable resolution. This paper presents calculations of the diffraction effects in an optical set-up using OTR. The OTR diffraction pattern in a telescopic system is calculated taking into account the radial polarization of OTR. The obtained diffraction pattern is compared to the patterns obtained by other authors and the effects of different parameters on the shape and on the size of the OTR diffraction pattern are studied. The major role played by the radial polarization on the shape of the diffraction pattern is outlined. An alternative method to calculate the OTR diffraction pattern is also sketched.

Keywords: Electromagnetic field calculations; Radiation; Electron beam devices; Instrumentation

* Corresponding author. Laboratoire de l'Accélérateur Linéaire, bat. 200, IN2P3-CNRS, Université de Paris-Sud, B.P. 34, F-91898 Orsay Cedex, France.
Fax: +33 1 69 07 14 99. E-mail: khonkava@lalcls.in2p3.fr.
† Presently at CERN.

1 INTRODUCTION

Optical transition radiation (OTR) provides an attractive method for beam diagnostics of charged particle beams and it has been used for that purpose in the keV–MeV energy region for electron beams and in the GeV region for proton beams. There have been, however, statements that the geometrical resolution of OTR might deteriorate drastically at high energies due to the diffraction phenomenon. Related to that, some authors[1] have put a limit on the geometrical resolution at a '$\gamma\lambda$' value, where γ is the Lorentz factor and λ the wavelength of observation. Several studies concerning the resolution of OTR (see Refs. [2–11]) have been published in the last years and this paper extends these investigations concentrating on the optical diffraction of OTR in a telescopic system.

In order to study the resolution of the OTR we shall calculate the diffraction pattern of OTR on the image plane of a telescope, which is situated in the direction of specular reflection of the incident particle (i.e. only the case of backward OTR is considered). Naturally, the results are valid on the image plane of any kind of imaging system. Scalar diffraction theory (see, for example, Ref. [12] or Ref. [13]) used by Rule and Fiorito in Refs. [3–5] does not take into account the polarization of the field. Precisely, in the case of OTR the polarization is important, since the polarization of OTR is not uniform, but radial (the electric field is in a plane containing the wave vector and the direction of the specular reflection). This can be taken into account by considering separately the horizontal and the vertical field components. The method is similar to that used by Hofmann and Méot in Ref. [14] for synchrotron radiation. Our treatment yields a satisfactory description of the diffraction phenomenon and provides a relatively simple, clear and straightforward method to compute the transition radiation diffraction pattern. The shape of the diffraction pattern calculated here is identical to that obtained by Lebedev in Ref. [9] and more recently by us in Ref. [10] and by Castellano and Verzilov in Ref. [11]. The OTR diffraction pattern will also be compared to the "scalar" pattern similar to that obtained by Rule and Fiorito in Refs. [3–5] and to the standard diffraction pattern (diffraction pattern of an ideal isotropic point source). The effect of the radial polarization alone will be studied by calculating the diffraction pattern of a source which is radially polarized, but having an isotropic intensity.

2 RECALLS

Before calculating the diffraction pattern of OTR in a telescopic system, we shall recall some basic characteristics of OTR and of the scalar diffraction theory.

2.1 Optical Transition Radiation

Transition radiation is emitted when a charged particle crosses a boundary between two media of different optical properties. The emission occurs both into the forward and backward hemispheres with respect to the separating surface. Here, we shall consider the case of a single boundary between a metal and vacuum. Due to metal opacity, only forward (resp. backward) OTR is observed when the electron moves from metal to vacuum (resp. vacuum to metal). If the surface is perfectly reflecting ($r = r_{\parallel} = r_{\perp} = -1$), the angular distribution is approximately given (in Gaussian units) by (see, for example, Ref. [15])

$$I(\theta) = \frac{\mathrm{d}^2 W}{\mathrm{d}\omega\, \mathrm{d}\Omega} = \frac{e^2}{\pi^2 c} \left(\frac{\theta}{\gamma^{-2} + \theta^2} \right)^2 \tag{1}$$

where θ is the angle with respect to the electron velocity (forward OTR) or to the direction of the specular reflection of that velocity (backward OTR). γ is the Lorentz factor of the electron, and Eq. (1) is valid for $\gamma \gg 1$ and $\theta \ll 1$. From now on we will consider the case of backward OTR (Figure 1).

The emitted electric field has two polarization components: one in the plane of observation ($\hat{z}_s \hat{n}$-plane in Figure 1) and the other one in the plane perpendicular to that. In the transverse plane perpendicular to the direction of specular reflection ($\hat{x}\hat{y}$-plane in Figure 1), the electric field is radially polarized and in that plane it can be decomposed into horizontal ($\hat{x}$-direction) and vertical ($\hat{y}$-direction) components.

2.2 Transformation of Image Fields by an Optical System in the Scalar Wave Diffraction Theory

Let us first consider a wave of frequency $\omega = (c/n)k$ propagating between two planes Π and Π' without any lenses between them. In the

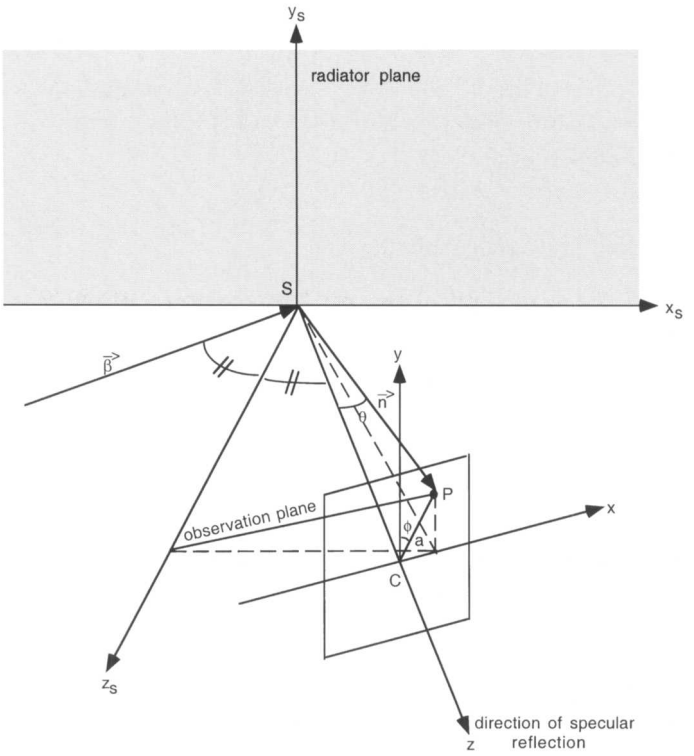

FIGURE 1 Definition of coordinates and planes.

scalar wave theory, with the approximation of Gaussian optics, the amplitude $\psi(P')$ in the plane Π' is related to the amplitude $\psi_0(P)$ in the plane Π by

$$\psi(P') = -\frac{\mathrm{i}}{\lambda}\int_{\Pi}\psi_0(P)\frac{\mathrm{e}^{\mathrm{i}kR}}{R}\,\mathrm{d}S \tag{2}$$

where R is the distance between points P and P'. The time-dependent factor $\mathrm{e}^{-\mathrm{i}\omega t}$ has been factored out both in ψ and ψ_0. We can treat the $(1/R)$-factor as a constant (in the Gaussian optics approximation) and write

$$\psi(P') = A\int_{\Pi}\psi_0(P)\mathrm{e}^{\mathrm{i}kR}\,\mathrm{d}S \tag{3}$$

where $A = \mathrm{i}/(\lambda L)$ and L is the distance between the two planes.

Let us now consider the case where one or several "non-diaphragmed" lenses are inserted between the planes Π and Π'. By "non-diaphragmed" lens, we mean a lens with an aperture much larger than the transverse size of the optical wave packet. Equation (3) can be generalized as*

$$\psi(P') = A \int_{\Pi} \psi_0(P) e^{ik\mathcal{L}(P,P')} \, dS \tag{4}$$

where $\mathcal{L}(P, P')$ is the optical distance between points P and P', i.e. the integral

$$\mathcal{L}(P, P') = \int_{P}^{P'} n \, dl \tag{5}$$

along the geometrical optical ray connecting P and P', n is the refractive index. A is a complex factor, which depends only on the location of the planes and which we will not calculate, since we are interested only in the shape of the OTR image.

3 DIFFRACTION EFFECT OF DIAPHRAGMS IN A TELESCOPE

In this section we consider diffraction effect caused by the diaphragms of a telescope, and in the next one we will take into account also the special properties of OTR.

We have taken the experimental set-up used in our experiment at Orsay[6] as the geometrical basis for the diffraction calculations. In this experiment backward OTR emitted by a 2 GeV electron beam was measured in the direction of the specular reflection. The set-up consisted of an OTR radiator, two lenses in *a telescopic configuration* and a CCD-camera; henceforth the CCD is referred to as a screen. The first lens had a focal length of 1 m and a diameter of 8 cm; the focal length of the second one was 25 cm and the diameter 14 cm. The first lens with a smaller diameter gives the effective aperture limitation of the system. The telescope geometry is presented in Figure 2.

* Equation (4) is applicable provided that the planes Π and Π' are not mutually conjugated.

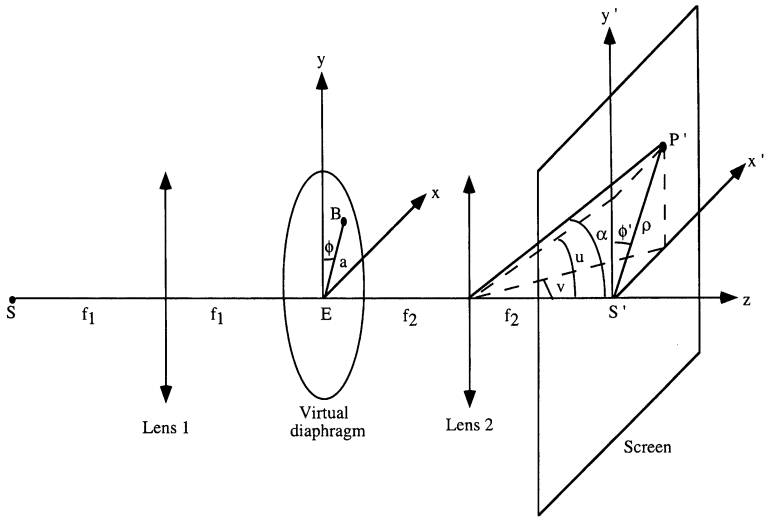

FIGURE 2 Schematic set-up.

We will treat the effect of the *real* diaphragm (at the first lens) in a slightly approximate but convenient way, replacing this diaphragm by a *virtual* one, with the same diameter, but located in the common focal plane between the lenses.† In that plane, the spatial coordinate a is directly related to the angle θ of the emitted radiation ($a = f_1\theta$) as resulting from the particular geometry of telescope.

Our observation point P' is situated in the image plane of the telescope (see Figure 2) and, according to Eq. (4), the modulus of the field at this point is related to the amplitude ψ_0 in the common focal plane by

$$|\psi(P')| = A\left|\int_{\epsilon} \psi_0(B) e^{ik\mathcal{L}(B,P')}\, d\epsilon\right| \tag{6}$$

where A is a normalization factor. The integration is performed over the aperture area ϵ of the virtual diaphragm.

The coordinates of a point B in the virtual diaphragm are $x = a\sin\phi$ and $y = a\cos\phi$ (Figure 2). In the image plane we use "prime"

† The real and the virtual diaphragms are in practice equivalent, when $a_0 \gg \gamma\lambda$ (the transverse size of the source) and $a_0/f_1 \gg \gamma^{-1}$ (the peak angle), where a_0 and f_1 are the radius and the focal length of the first lens. These two conditions are fulfilled in the following calculations.

coordinates: $x' = \rho \sin \phi'$ and $y' = \rho \cos \phi'$. The angular directions v and u in the small angle approximation can be written as

$$v = \frac{x'}{f_2} = \frac{\rho}{f_2} \sin \phi' = \alpha \sin \phi', \tag{7}$$

$$u = \frac{y'}{f_2} = \frac{\rho}{f_2} \cos \phi' = \alpha \cos \phi'. \tag{8}$$

In the phase factor of Eq. (6) we are interested in the relative phase difference. All the rays leaving the diaphragm in a particular direction are focused by the second lens into the same point of the screen (see Figure 3). According to the theorem of Malus,[16] all the rays perpendicular to a given surface (BF in Figure 3) have an equal optical path length from the surface to the focus point (point P' in Figure 3), and thus the optical path difference between the rays EAP' and BDP' is $d = |EF|$. This distance is the projection of the vector $\overrightarrow{EB}$ onto the direction of vector $\overrightarrow{EA}$: $d = |\overrightarrow{EB} \cdot (\overrightarrow{EA}/|\overrightarrow{EA}|)| = vx + uy$, where x and y are the coordinates of point B and v and u are the angular directions given by Eqs. (7) and (8), respectively. The corresponding phase difference can now be written as $\delta = -kd = -k(vx + uy)$. In polar coordinates the last paranthesis can be written as

$$vx + uy = \frac{x'}{f_2} x + \frac{y'}{f_2} y = \frac{\rho}{f_2} a \cos(\phi - \phi'). \tag{9}$$

Since OTR is symmetrical about the z-axis, there is no preferred value of the angle ϕ', and we may select $\phi' = 0$ and write the modulus of the diffracted amplitude in the point P' on the screen as

$$|\psi(P')| = A \left| \int_0^{2\pi} \int_0^{a_0} \psi_0(a, \phi) \exp\left(-\mathrm{i} \frac{2\pi}{\lambda} \frac{\rho}{f_2} a \cos \phi \right) a \, \mathrm{d}a \, \mathrm{d}\phi \right| \tag{10}$$

where $k = 2\pi/\lambda$ and $\psi_0(a, \phi)$ is the amplitude of the wave in the intermediate focal plane. The integration is made in polar coordinates and a_0 is the radius of the smaller lens (the limiting aperture of the system). It should be noticed that Eq. (10) is a particular form of a

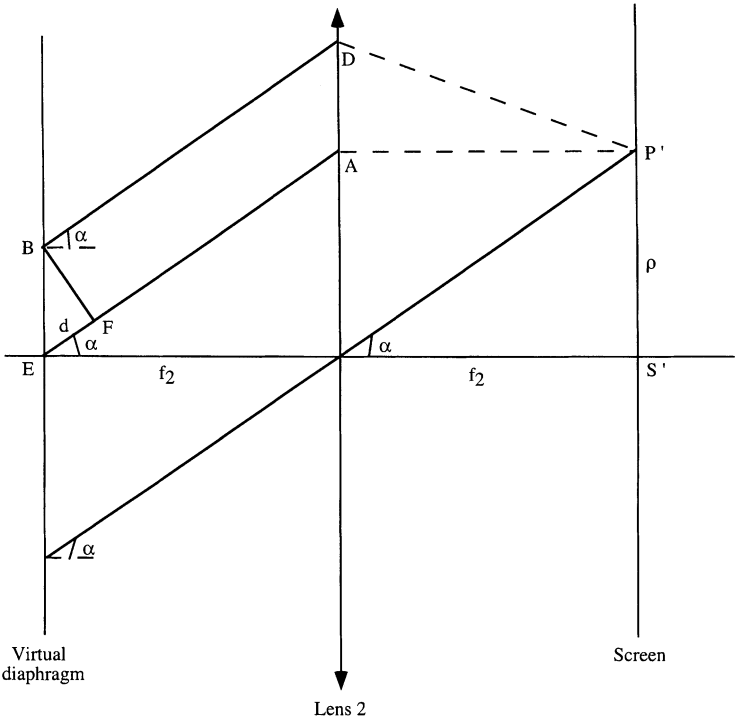

FIGURE 3 Sketch of rays after the virtual diaphragm.

two-dimensional Fourier transform of the wave amplitude ψ_0. We can therefore say, in agreement with Ref. [17, Chap. 5, Section 5.2.2], that the field in the image focal plane of the lens L_2 is proportional to the Fourier transform of the field in the object focal plane of L_2. In our derivation, this property appears essentially as a consequence of the Malus theorem.

4 DIFFRACTION OF OTR IN THE TELESCOPE

In the calculation of the diffraction pattern of OTR (i.e. the OTR spot in the image plane of the telescope) we need to consider both the amplitude and the polarization of the incident wave.

The scalar diffraction theory can be used without modification for the vector case if the direction of the field is the same in each point on the

diaphragm. The electric field of transition radiation is, however, radially polarized i.e. at different azimuthal angles ϕ the field vector has a different direction (it is always pointing to the center of symmetry). We may take this characteristic into account by considering separately the horizontal and vertical field components. The total intensity is the sum of the intensities from these two components.

When we decompose transition radiation into plane waves with directions of θ, the vector amplitude is proportional to $\vec{\theta}/(\gamma^{-2}+\theta^2)$, where $\vec{\theta} = \overrightarrow{CP}/|SC|$ (Figure 1). When considering the two polarization components separately, $\vec{\theta}$ can be replaced by $(\theta \sin\phi)$ for the horizontal and by $(\theta\cos\phi)$ for the vertical component.[‡] The phase of these plane waves is precisely zero in the electron impact point S.

A plane wave, whose direction of propagation has an angle θ with respect to the direction of specular reflection and whose azimuthal angle is ϕ, is focused to the point $B=(a,\phi)$ on the virtual diaphragm (where $\theta = a/f_1$) and the modulus of the electric field amplitude in this point is given by

$$|E_\omega(B)| = C' \frac{(a/f_1)}{\gamma^{-2}+(a/f_1)^2} \tag{11}$$

where f_1 is the focal length of the first lens and C' is a constant that takes into account the normalization and units.

When considering horizontal and vertical components separately, $|E_\omega(B)|$ has to be multiplied by the factor $(\sin\phi)$ or $(\cos\phi)$, respectively, and we can write

$$\psi_{0h}(a,\phi) = |E_\omega(B)|\sin\phi, \tag{12}$$

$$\psi_{0v}(a,\phi) = |E_\omega(B)|\cos\phi \tag{13}$$

where $\psi_{0h}(a,\phi)$ refers to the horizontal component and $\psi_{0v}(a,\phi)$ to the vertical one. We should multiply Eqs. (12) and (13) by a phase factor corresponding to the propagation between S and B. However, because E and B are on the same wave surface, the optical paths SE and SB are equal (invoking the Malus theorem), and if we forget the constant phase

[‡] Here the polar angle ϕ is defined with respect to the vertical axis.

factor, we do not have any extra phase factors to add into Eqs. (12) and (13).[§]

The total intensity at the point P' is the sum of the intensities from the horizontal and the vertical components:

$$I(P') = |\mathcal{E}(P')|^2 = |\mathcal{E}(P')|_h^2 + |\mathcal{E}(P')|_v^2. \tag{14}$$

In the case of OTR in a telescope, $|\mathcal{E}(P')|_h$ and $|\mathcal{E}(P')|_v$ are obtained by substituting Eqs. (12) and (13) into Eq. (10). By using the expression given by Eq. (11), we obtain

$$|\mathcal{E}(P')|_h = A' \left| \int_0^{a_0} \int_0^{2\pi} \frac{(a/f_1)\sin\phi}{\gamma^{-2} + (a/f_1)^2} \exp\left(-i\frac{2\pi}{\lambda}\frac{\rho}{f_2} a\cos\phi\right) a\,da\,d\phi \right|, \tag{15}$$

$$|\mathcal{E}(P')|_v = A' \left| \int_0^{a_0} \int_0^{2\pi} \frac{(a/f_1)\cos\phi}{\gamma^{-2} + (a/f_1)^2} \exp\left(-i\frac{2\pi}{\lambda}\frac{\rho}{f_2} a\cos\phi\right) a\,da\,d\phi \right| \tag{16}$$

where A' is a normalization constant.

The integration over ϕ in the horizontal component gives zero, thus only the vertical component contributes to the total intensity, and we obtain

$$I(P') = |\mathcal{E}(P')|_v^2 = C \left| \int_0^{a_0} \frac{a^2}{\gamma^{-2} + (a/f_1)^2} J_1\left(\frac{2\pi}{\lambda}\frac{\rho}{f_2} a\right) da \right|^2 \tag{17}$$

where J_1 is the first order Bessel function and C a generic normalization constant.

We have defined the azimuthal angles ϕ and ϕ' with respect to the vertical axis. If we had defined them with respect to the horizontal axis, we would have interchanged the $\sin\phi$ and $\cos\phi$-factors in Eqs. (12) and (13) leading to same result for the total intensity.

[§] The plane wave decomposition of OTR is proportional to the two-dimensional Fourier transform of the OTR field at the radiator. Therefore, Eq. (11), like Eq. (10), can be considered as an application of Ref. [17, Chapter 5, Section 5.2.2], the lens being in this case L_1.

When the observer is on the vertical axis, he sees only the vertical polarization. If he is placed on the horizontal axis, he sees only the horizontal polarization.

The integration over a in Eq. (17) can be performed numerically and the result as a function of the radius ρ on the screen is shown in Figure 4 for our experimental conditions ($E = 2\,\text{GeV}$, $f_1 = 1\,\text{m}$, $f_2 = 25\,\text{cm}$, $a_0 = 4\,\text{cm}$, $\theta_1 = a_0/f_1 = 40\,\text{mrad}$, $\lambda = 500\,\text{nm}$). This distribution, which represents the diffraction pattern of an OTR source taking into account the radial polarization, is shown around the symmetry axis. Since we are not interested in the absolute intensity, the peak intensity is normalized to unity. The magnification of the used telescope is $M = f_2/f_1 = 0.25$; if we use an imaging system with magnification of one, the diffraction pattern is naturally four times wider. The FWHM size of the pattern in Figure 4 is about 4.5 μm (FWHM ≈ 18 μm, when

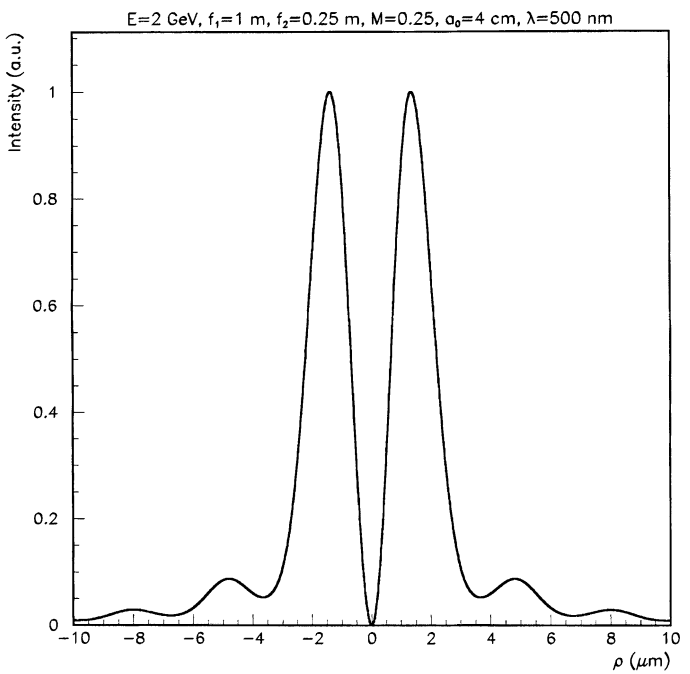

FIGURE 4 OTR diffraction pattern (intensity) around the symmetry axis on the image plane of a telescope with magnification $M = 0.25$ ($E = 2\,\text{GeV}$, $f_1 = 1\,\text{m}$, $f_2 = 25\,\text{cm}$, $M = f_2/f_1 = 0.25$, $a_0 = 4\,\text{cm}$, $\theta_1 = a_0/f_1 = 40\,\text{mrad}$, $\lambda = 500\,\text{nm}$). In a one-to-one imaging system the size of the diffraction pattern is four times larger.

$M = 1$). This pattern shape is in full agreement with that of Lebedev obtained in Ref. [9]. Similar observations concerning this pattern shape are presented in Refs. [10] and [11].

4.1 Effects of Different Parameters on the OTR Diffraction Pattern

Next we study the effects of different parameters on the OTR diffraction pattern. Since we are only interested in the size of the pattern, the peak intensities are always scaled to unity. In all the figures the magnification of the system is 0.25; when using a one-to-one imaging system, the patterns are four times wider.

Figure 5 shows the OTR diffraction pattern for different wavelengths. We can see, as expected, that the size of the pattern scales proportionally to the wavelength. The resolution can be improved when using smaller wavelengths, but if we are out of the optical range ($\lambda \lesssim$ 350 nm), we cannot use an optical imaging system and the experimental conditions become more complicated.

In Figure 6 the geometrical size of the aperture (a_0) is varied. Naturally, the decrease of the aperture size causes an enlargement of the diffraction pattern.

Figure 7 shows OTR diffraction pattern for different energies in the GeV energy range. The FWHM size of the distribution is independent of γ. The difference is in the tails: the higher is the energy, the stronger are the tails.

In Refs. [2,6,18] and more recently also in Refs. [10] and [11], it has been considered a possibility to use a mask,[¶] which removes the small angles (i.e. the γ^{-1} peak), to improve the spatial resolution. The effect of a mask can be taken into account by introducing into Eq. (17) an extra pupil function representing the cut caused by the mask. It amounts to setting the lower limit of integration in Eq. (17) to a_m instead of zero, where a_m is the radius of the mask.[‖] A mask reduces the tails, as can be seen in Figure 8, where OTR diffraction pattern for $E = 10\,\text{GeV}$

[¶] A "stop" in Ref. [2].

[‖] The mask should, in principle, be put in the common focal plane of lenses L_1 and L_2. However, it can be put on L_1, if $a_m \gg \gamma\lambda$ and $(a_m/f_1) \gg \gamma^{-1}$ (cf. similar conditions than for the real diaphragm).

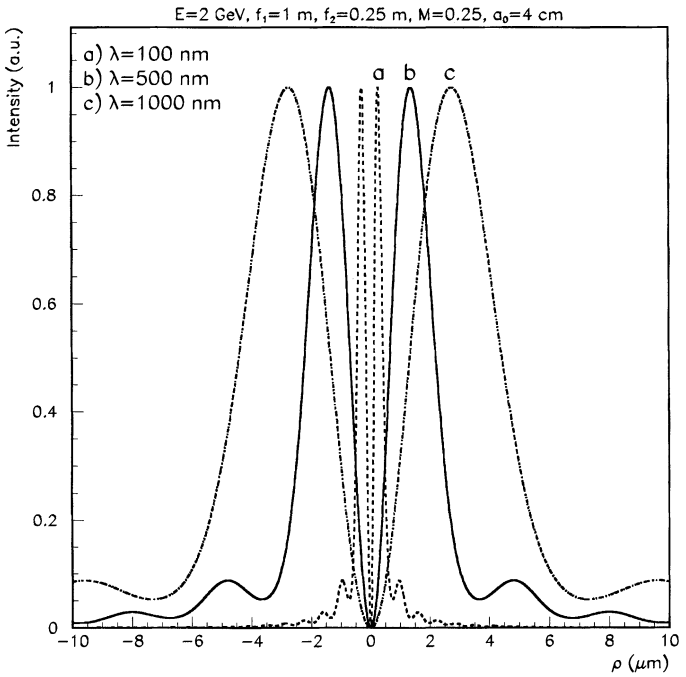

FIGURE 5 OTR diffraction pattern for different wavelengths (a) $\lambda = 100\,\text{nm}$, (b) $\lambda = 500\,\text{nm}$ and (c) $\lambda = 1\,\mu\text{m}$ on the image plane of a telescope with magnification $M = 0.25$. The used parameters are the same as in Figure 4.

($M = 0.25$) has been plotted with and without a mask ($a_m = 2\,\text{mm}$). However, it does not affect significantly the FWHM size of the pattern.

4.2 Diffraction of a Gaussian Emitter

So far, we have considered OTR emitted by a single electron. Diffraction of OTR emitted by a Gaussian beam can be treated by convoluting on the image plane the OTR diffraction pattern and a Gaussian distribution, which is the image of the beam distribution. This is a two-dimensional convolution:

$$I_{\text{conv}}(x, y) = \int\int I(x - x_1, y - y_1)\mathcal{O}(x_1, y_1)\mathrm{d}x_1\,\mathrm{d}y_1 \qquad (18)$$

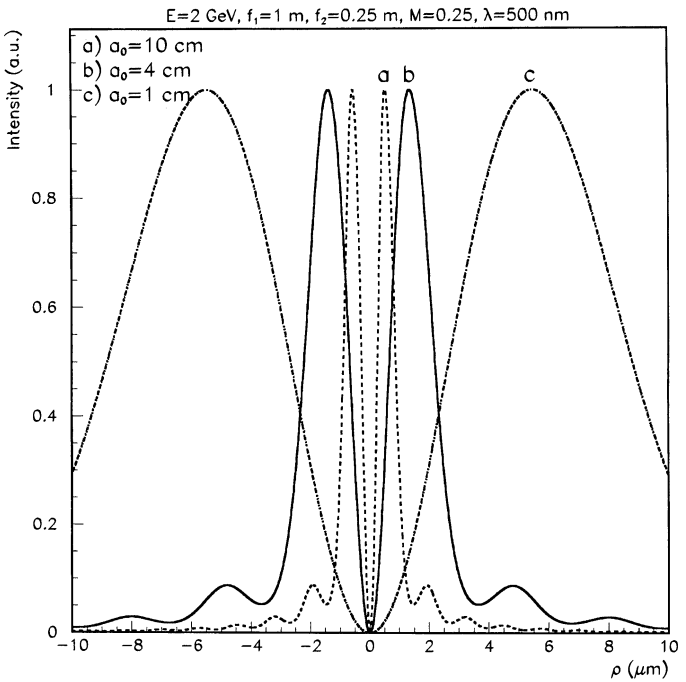

FIGURE 6 OTR diffraction pattern for different geometrical aperture sizes (a) $a_0 = 10\,\text{cm}$, (b) $a_0 = 4\,\text{cm}$ and (c) $a_0 = 1\,\text{cm}$ on the image plane of a telescope with magnification $M = 0.25$. The used parameters are the same as in Figure 4.

where $I(x, y)$ is the OTR diffraction pattern (Eq. (17)) in cartesian coordinates ($\rho = \sqrt{x^2 + y^2}$) and $\mathcal{O}(x, y)$ the image of the beam profile:

$$\mathcal{O}(x, y) = \frac{1}{\sqrt{2\pi}\sigma_{ix}} \exp\left(-\frac{x^2}{2\sigma_{ix}^2}\right) \frac{1}{\sqrt{2\pi}\sigma_{iy}} \exp\left(-\frac{y^2}{2\sigma_{iy}^2}\right) \tag{19}$$

where σ_{ix} and σ_{iy} are the horizontal and vertical rms sizes of the Gaussian beam image.

5 COMPARISON WITH STANDARD DIFFRACTION

Let us calculate for comparison the diffraction pattern of an ideal isotropic point source (the standard diffraction pattern) in a telescope.

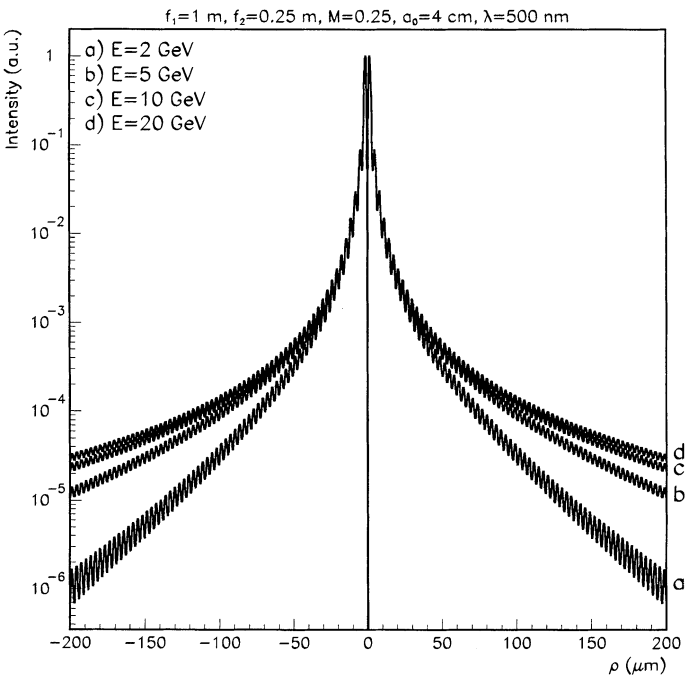

FIGURE 7 OTR diffraction pattern for different energies (a) $E=2\,\text{GeV}$, (b) $E=5\,\text{GeV}$, (c) $E=10\,\text{GeV}$ and (d) $E=20\,\text{GeV}$ on the image plane of a telescope with magnification $M=0.25$. The used parameters are the same as in Figure 4.

In that case $\psi_0(a,\phi)=\text{constant}$. By substituting this into Eq. (10) and squaring, we obtain

$$I(P') = \text{const} * \left| \int_0^{2\pi} \int_0^{a_0} \exp\left(-\text{i}\frac{2\pi}{\lambda}\frac{\rho}{f_2} a\cos\phi\right) a\,\text{d}a\,\text{d}\phi \right|^2. \tag{20}$$

Integration over ϕ and a gives

$$I(P') = C\left|\frac{J_1([(2\pi\rho)/(\lambda f_2)]a_0)}{([(2\pi\rho)/(\lambda f_2)]a_0)}\right|^2 \tag{21}$$

where J_1 is the first order Bessel function and C is a generic normalization constant.

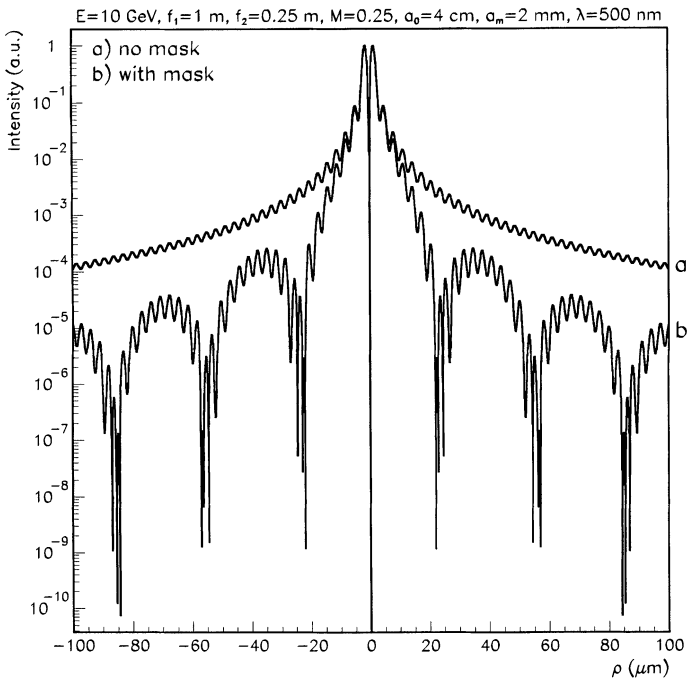

FIGURE 8 Effect of a mask with a radius $a_m = 2\,\text{mm}$ ($a_m/a_0 = 0.05$). $E = 10\,\text{GeV}$; the used parameters are the same as in Figure 4.

In Figure 9 the standard diffraction pattern given by Eq. (21) (curve a) is compared with the OTR diffraction pattern given by Eq. (17) (curve c) in our experimental conditions. The peak intensities are both normalized to unity. We can see that the OTR diffraction pattern is wider (the FWHM size is about 2.7 times that of the standard diffraction pattern) and has a zero in the center.

6 DIFFRACTION OF "SCALAR OTR"

If we do not take into account the radial polarization of OTR, but only the angular distribution of it, we can use the right hand side of Eq. (11)

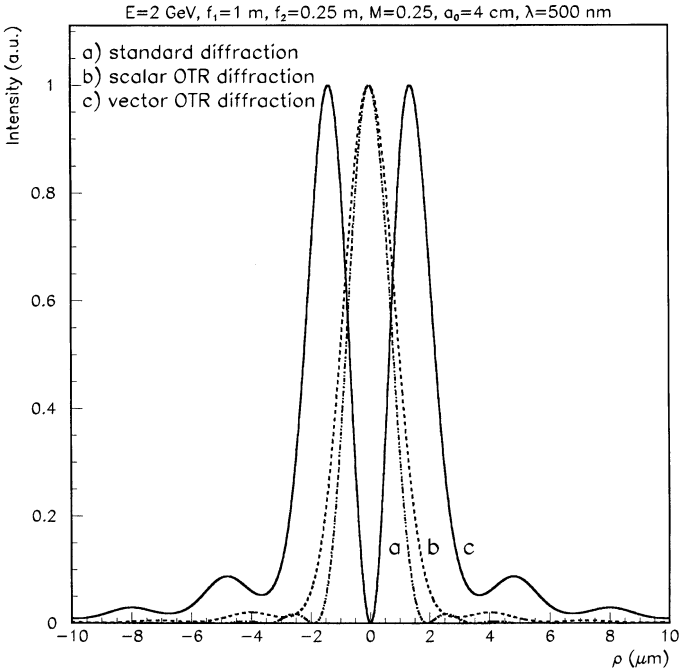

FIGURE 9 Standard diffraction pattern given by Eq. (21) (curve a), "vector" OTR diffraction pattern given by Eq. (17) (curve c) and "scalar" OTR diffraction pattern given by Eq. (23) (curve b) on the image plane of a telescope with magnification $M = 0.25$. The used parameters are the same as in Figure 4.

as the algebraic amplitude. By substituting it into Eq. (10) we obtain

$$|\mathcal{E}(P')| = A' \left| \int_0^{2\pi} \int_0^{a_0} \frac{(a/f_1)}{\gamma^{-2} + (a/f_1)^2} \exp\left(-\mathrm{i} \frac{2\pi}{\lambda} \frac{\rho}{f_2} a \cos\phi \right) a \, \mathrm{d}a \, \mathrm{d}\phi \right|. \tag{22}$$

After integrating over ϕ we have

$$I(P') = |\mathcal{E}(P')|^2 = C \left| \int_0^{a_0} \frac{a^2}{\gamma^{-2} + (a/f_1)^2} J_0\left(\frac{2\pi}{\lambda} \frac{\rho}{f_2} a \right) \mathrm{d}a \right|^2 \tag{23}$$

where J_0 is the zero order Bessel function and C is a generic normalization constant.

The integration over a can again be performed numerically and the resulting diffraction pattern is plotted in Figure 9 (curve b). The peak intensity is again normalized to unity. This pattern is similar to the pattern obtained by Rule and Fiorito in Refs. [3–5]. The FWHM size of this "scalar OTR" diffraction pattern is by a factor of ~ 1.2 wider than the FWHM size of the standard diffraction pattern; the FWHM size of the "vector OTR" pattern given by Eq. (17) is by a factor of ~ 2.2 wider than the FWHM size of the "scalar" one (Eq. (23)).

7 IMPORTANCE OF THE RADIAL POLARIZATION IN THE DIFFRACTION PHENOMENON

For a field which is invariant by rotation about the direction of the specular reflection, the amplitude distribution and the polarization of the field can be described by separate functions $\mathcal{A}$ and $\mathcal{F}$, respectively. According to Eq. (10) we can write

$$|\mathcal{E}(P')|_j = A\left|\int_0^{2\pi}\int_0^{a_0} \mathcal{A}(a)\mathcal{F}_j(\phi)\exp\left(-\mathrm{i}\frac{2\pi}{\lambda}\frac{\rho}{f_2}a\cos\phi\right)a\,\mathrm{d}a\,\mathrm{d}\phi\right| \quad (24)$$

where index j refers to the horizontal or to the vertical component. The total intensity is the sum of the intensities from different components: $I(P') = \sum_j |\mathcal{E}(P')|_j^2$.

When the field is radially polarized, the polarization function is $\mathcal{F}_\mathrm{h}(\phi) = \sin\phi$ for the horizontal component and $\mathcal{F}_\mathrm{v}(\phi) = \cos\phi$ for the vertical one. The angle ϕ is again defined with respect to the vertical axis. Let us consider a hypothetical case in which the field is constant in the amplitude: $\mathcal{A}(a) = \text{constant}$. By substituting these into Eq. (24), we obtain

$$|\mathcal{E}(P')|_\mathrm{h} = \text{const} * \left|\int_0^{2\pi}\int_0^{a_0} \sin\phi\exp\left(-\mathrm{i}\frac{2\pi}{\lambda}\frac{\rho}{f_2}a\cos\phi\right)a\,\mathrm{d}a\,\mathrm{d}\phi\right|, \quad (25)$$

$$|\mathcal{E}(P')|_\mathrm{v} = \text{const} * \left|\int_0^{2\pi}\int_0^{a_0} \cos\phi\exp\left(-\mathrm{i}\frac{2\pi}{\lambda}\frac{\rho}{f_2}a\cos\phi\right)a\,\mathrm{d}a\,\mathrm{d}\phi\right|. \quad (26)$$

The integration over ϕ in the horizontal component gives again zero and we obtain for the total intensity

$$I(P') = |\mathcal{E}(P')|_{\mathrm{v}}^2 = C\left|\int_0^{a_0} aJ_1\left(\frac{2\pi}{\lambda}\frac{\rho}{f_2}a\right)\mathrm{d}a\right|^2 \tag{27}$$

where C is a generic normalization constant.

Equation (27) is plotted in Figure 10 (curve a) together with the OTR diffraction pattern (curve b). The peak intensities are both normalized to unity. It is important to understand that the peculiar shape of the OTR diffraction pattern in the central region with a zero in the center is essentially determined by the radial polarization. The non-constant angular distribution of OTR only widens the pattern a little: the FWHM value is wider by a factor of ~ 1.2, when the OTR angular distribution is taken into account.

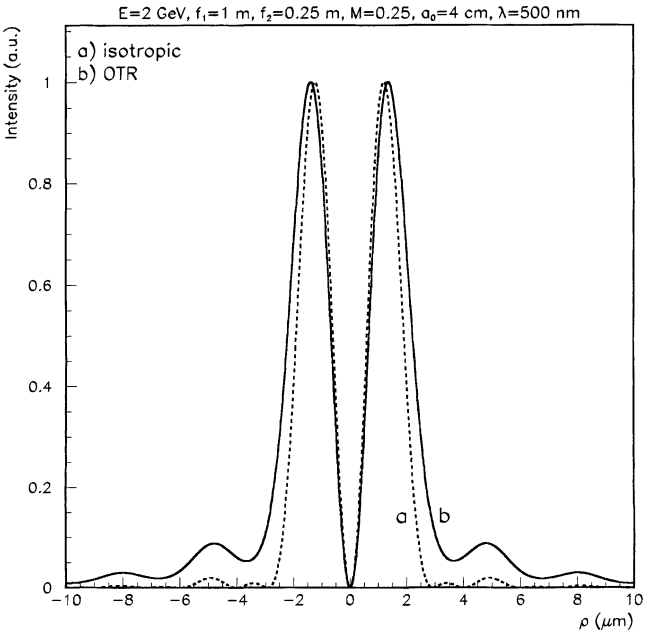

FIGURE 10 Diffraction pattern on the image plane of a telescope with magnification $M = 0.25$ given by radial polarization: (a) isotropic angular distribution (Eq. (27)) and (b) OTR angular distribution (Eq. (17)). The used parameters are the same as in Figure 4.

8 ANOTHER TREATMENT OF OTR DIFFRACTION

Diffraction of OTR can also be studied from a more theoretical point of view. A detailed treatment of this kind is presented elsewhere[10] and here we only shortly show that we can obtain, using this method, the same expression for diffraction pattern as obtained in Section 4.

The angular distribution of transition radiation in natural rational units ($c = \hbar = \epsilon_0 = 1$, $e^2/4\pi = \alpha = 1/137$) can be written as

$$I(\omega, \theta) = \omega \frac{dN}{d\omega\, d\Omega} \simeq \frac{\alpha}{\pi^2} \left(\frac{\theta}{\gamma^{-2} + \theta^2} \right)^2 . \tag{28}$$

In the case of forward radiation, Eq. (28) is the spectrum emitted by a suddenly accelerated electron and in the backward case the spectrum emitted by a suddenly stopped "image positron". The radiation field (in the far-field region) can be decomposed in plane waves

$$\mathbf{E}(t, \vec{\mathbf{r}}) = \int \frac{d^3\vec{\mathbf{k}}}{(2\pi)^3} \tilde{\mathbf{E}}(\vec{\mathbf{k}}) e^{i\vec{\mathbf{k}}\cdot\vec{\mathbf{r}} - i|\vec{\mathbf{k}}|t} \tag{29}$$

with

$$\tilde{\mathbf{E}}(\vec{\mathbf{k}}) \simeq ie \frac{\vec{\mathbf{q}}}{\vec{\mathbf{q}}^2 + \gamma^{-2} k_L^2} \tag{30}$$

where $\vec{\mathbf{q}}$ and $\vec{\mathbf{k}}_L$ are the transverse and the longitudinal components of the wave vector $\vec{\mathbf{k}}$, respectively.

The impact parameter profile** is related to the $\vec{\mathbf{q}}$-Fourier transform of $\tilde{\mathbf{E}}$:

$$\begin{aligned} I(\vec{\mathbf{b}}) &\equiv \frac{\omega\, dN}{d\omega\, d^2\vec{\mathbf{b}}} \simeq \frac{1}{\pi} \left| \mathbf{E}(\omega, \vec{\mathbf{b}}) \right|^2 \\ &= 4\alpha \left| \int \frac{d^2\vec{\mathbf{q}}}{(2\pi)^2} \frac{\vec{\mathbf{q}}}{\vec{\mathbf{q}}^2 + q_0^2} f(q) e^{i\vec{\mathbf{q}}\cdot\vec{\mathbf{b}}} \right|^2 \end{aligned} \tag{31}$$

** The impact parameter $\vec{\mathbf{b}}$ is defined as the transverse distance of the photon to the electron trajectory (forward OTR) or to the "image positron" trajectory (backward OTR) and $b = |\vec{\mathbf{b}}|$ is related to the radial coordinate ρ in the image plane by $b = \rho/M$; M is the magnification of the optical system.

where $f(q)$ is a cut-off function:

$$f(q) = \Theta(q - q_{\mathrm{m}})\Theta(q_1 - q). \tag{32}$$

The parameters q_0, q_1 and q_{m} are defined as

$$q_0 = \gamma^{-1} k_{\mathrm{L}} \simeq \gamma^{-1}\omega, \tag{33}$$

$$q_1 = \theta_1 \omega, \tag{34}$$

$$q_{\mathrm{m}} = \theta_{\mathrm{m}}\omega, \tag{35}$$

where θ_1 is the upper cut-off angle determined by some diaphragm and θ_{m} the lower cut-off angle determined by some mask. If no mask is used, $\theta_{\mathrm{m}} = 0 \rightarrow q_{\mathrm{m}} = 0$.

Using the properties of Bessel functions Eq. (31) can be developed as

$$\begin{aligned} I(b) &= 4\alpha \left| \int\int \frac{\mathrm{d}^2\vec{\mathbf{q}}}{(2\pi)^2} \frac{\vec{\mathbf{q}}}{\vec{\mathbf{q}}^2 + q_0^2} f(q) \mathrm{e}^{\mathrm{i}\vec{\mathbf{q}}\cdot\vec{\mathbf{b}}} \right|^2 \\ &= 4\alpha \left| \vec{\nabla}_{\vec{\mathbf{b}}} \int\int \frac{\mathrm{d}^2\vec{\mathbf{q}}}{(2\pi)^2} \frac{f(q)}{\vec{\mathbf{q}}^2 + q_0^2} \mathrm{e}^{\mathrm{i}\vec{\mathbf{q}}\cdot\vec{\mathbf{b}}} \right|^2 \\ &= \frac{\alpha}{\pi^2} \left| \vec{\nabla}_{\vec{\mathbf{b}}} \int q \, \mathrm{d}q \frac{f(q)}{q^2 + q_0^2} J_0(qb) \right|^2 \\ &= \frac{\alpha}{\pi^2} \left| \int q^2 \, \mathrm{d}q \frac{f(q)}{q^2 + q_0^2} J_1(qb) \right|^2 . \end{aligned} \tag{36}$$

If we substitute for $f(q)$, the sharp cut-off function Eq. (32), we obtain

$$I(b) = \frac{\alpha}{\pi^2} \left| \int_{q_{\mathrm{m}}}^{q_1} \frac{q^2}{q^2 + q_0^2} J_1(qb) \mathrm{d}q \right|^2 . \tag{37}$$

This can be written using the angle $\theta = q\lambda\!\!\!^{-}$ and $q_0 = \gamma^{-1}\lambda\!\!\!^{-1}$ (in natural units $\omega = \lambda\!\!\!^{-1}$)as

$$I(b) = C_1 \left| \int_{\theta_{\mathrm{m}}}^{\theta_1} \frac{\theta^2}{\theta^2 + \gamma^{-2}} J_1\left(\frac{\theta}{\lambda\!\!\!^{-}} b\right) \mathrm{d}\theta \right|^2 . \tag{38}$$

If we rewrite the diffraction pattern given by Eq. (17) using $a = f_1\theta$, $M =$ magnification $= f_2/f_1$ and the integration limits $\theta_1 = a_0/f_1$ and $\theta_m = a_m/f_1$ (i.e. we have a mask), we obtain

$$I(\rho) = C_2 \left| \int_{\theta_m}^{\theta_1} \frac{\theta^2}{\gamma^{-2} + \theta^2} J_1\left(\frac{2\pi}{\lambda}\frac{\theta}{M}\rho\right) \mathrm{d}\theta \right|^2 \tag{39}$$

We can see that this is identical (excluding the constant factor) to Eq. (38) taking into account the image magnification $\rho = Mb$.

9 HIGH ENERGY OTR EXPERIMENTS

In order to study experimentally the spatial resolution of OTR, three groups have carried out high energy OTR experiments. During 1995–1996 our group measured at the Orsay linear accelerator backward OTR emitted by a 2 GeV electron beam crossing an aluminum foil.[6] Almost simultaneously there was an experiment at CEBAF (Thomas Jefferson Laboratory, Virginia) by Denard *et al.* using forward OTR from ~ 4 GeV electrons.[7] More recently backward OTR emitted by 22 GeV electrons have been measured by Jung *et al.* at CERN.[8]

In all these experiments rms beam widths smaller than '$\gamma\lambda$' have been measured. The ratios (marked here by η) between the '$\gamma\lambda$' value and the rms width in the different experiments were: $\eta \sim 2$ at Orsay (2 GeV), $\eta \sim 5$ at CEBAF (3.2 GeV) and $\eta \sim 3$ at CERN (22 GeV). These ratios are obviously depending on the ability of obtaining very small beam dimensions in a given optical channel of the accelerator.

10 SUMMARY AND CONCLUSIONS

In this paper, we have considered the limitations brought by the diffraction to the resolution of OTR images of high energy charged particles. Starting from the scalar wave theory, some basic formulas concerning the wave propagation in an optical system were recalled. Choosing, for

the optical system, a telescope which exhibits very simple and interesting properties, we have calculated the diffraction pattern of the OTR wave emitted by one electron. A virtual diaphragm, located in the common focal plane between the lenses of the telescope, allowed us to express the diffraction in a rather simple way. The radial polarization of OTR was taken into account by considering the horizontal and vertical field components separately.

Our results coincide with those of Lebedev[9] and they are in qualitative agreement with those of Rule and Fiorito obtained in the scalar wave approximation.[3–5] The obtained diffraction pattern was also compared to the well known standard diffraction pattern. The FWHM size of the OTR diffraction pattern is about two times wider than that of the "scalar OTR" pattern and about three times wider than that of the standard diffraction pattern.

Consideration of the general shape of the OTR diffraction pattern shows that the FWHM width is insensitive for the particle energy, whereas the tails increase with the energy. These tails may be seen by very sensitive detectors: in that case, a central optical mask constitutes an effective cure.

The high energy OTR experiments in three laboratories, at different energies, have also shown that the resolution limit is well below the '$\gamma\lambda$' value.

In conclusion, up to energies considered ($\gamma \sim 5 * 10^4$), the effects of the diffraction, evaluated by the FWHM of the OTR diffraction pattern, are not limiting the resolution. The resolution depends more likely on the properties of the experimental set-up, the contrast sensitivity of the detector and the data treatment procedure.

References

[1] K.T. McDonald and D.P. Russell, "Methods of emittance measurement", *Proc. Joint US-CERN School on Observation, Diagnosis and Correction in Particle Beams*, October 1988, Capri.

[2] E.W. Jenkins, "Optical transition radiation from a thin carbon foil – A beam profile monitor for the SLC", Single Pass Collider Memo CN-260 (1983).

[3] D.W. Rule and R.B. Fiorito, "Imaging micron sized beams with optical transition radiation", *A.I.P. Conf. Proc. No. 229* (1991) 315.

[4] D.W. Rule and R.B. Fiorito, "Beam profiling with optical transition radiation", *Proc. 1993 Particle Accelerator Conf.*, May 1993, Washington DC, p. 2453.

[5] R.B. Fiorito and D.W. Rule, 1993 Faraday Cup Award Invited Paper, *Proc. Beam Instrumentation Workshop, Conf. Proc. No. 319* (1994) 21.

[6] X. Artru *et al.*, "Experimental investigations on geometrical resolution of optical transition radiation (OTR)", *Nucl. Inst. Meth.* **A410** (1998) 148.
[7] J.-C. Denard *et al.*, "High power beam profile monitor with optical transition radiation", *Proc. 1997 Particle Accelerator Conf.*, May 1997, Vancouver, p. 2198.
[8] D. Giove *et al.*, "Optical transition radiation diagnostics", *Proc. DIPAC 97*, October 1997, Frascati, LNF-97/048(IR), p. 251.
[9] V.A. Lebedev, "Diffraction-limited resolution of the optical transition radiation monitor", *Nucl. Inst. Meth.* **A372** (1996) 344.
[10] X. Artru *et al.*, "Resolution power of optical transition radiation: Theoretical considerations", *Nucl. Inst. Meth.* **B145** (1998) 160 (RREPS'97 symposium, September 1997, Tomsk).
[11] M. Castellano and V.A. Verzilov, "Spatial resolution in optical transition radiation (OTR) beam diagnostics", *Phys. Rev. ST Accel. Beams* **1** (1998) 062801.
[12] M. Born and E. Wolf, *Principles of Optics*, Third (revised) edition, Pergamon Press, 1965.
[13] L.D. Landau and E.M. Lifshitz, *The Classical Theory of Fields*, Revised second edition, Pergamon Press, 1962.
[14] A. Hofmann and F. Méot, "Optical resolution of beam cross-section measurements by means of synchrotron radiation", *Nucl. Inst. Meth.* **203** (1982) 483.
[15] L. Wartski, Thése de doctorat d'Etat, Univ. Paris-Sud (1976).
[16] W.T. Welford, *Geometrical Optics*, Optical Instrumentation, Vol. 1, North-Holland, 1962.
[17] J.W. Goodman, *Introduction to Fourier Optics*, McGraw-Hill, 1996.
[18] S.D. Borovkov *et al.*, "On studying a possibility to use optical transition radiation for proton beam diagnostics", *Nucl. Inst. Meth.* **A294** (1990) 101.